

Article

# The Effect of Void on the

Firstname Lastname<sup>1,†,‡</sup>, Firstname Lastname<sup>1,‡</sup> and Firstname Lastname<sup>2,\*</sup>

<sup>1</sup> School of Mechanical and Electronical Engineering, Lanzhou University of Technology, Lanzhou 730050, China; e-mail@e-mail.com

<sup>2</sup> Affiliation 2; e-mail@e-mail.com

\* Correspondence: e-mail@e-mail.com; Tel.: +x-xxx-xxx-xxxx

† Current address: Affiliation 3

‡ These authors contributed equally to this work.

Version October 4, 2018 submitted to Journal Not Specified

**Abstract:** Fracture processes of nanocrystalline metallic materia is affected by dislocation, nanovoid and other defects. Existing studies of defect evolution in titanium-aluminium alloy cover the case that voids located in single crystals, inside grain in poly crystals and at the grain boundaries. Molecular dynamics simulation was performed to study the evolution of a spherical nanovoid in  $\alpha+\gamma$  two-phase titanium-aluminium alloy under uniaxial tension. The results show that voids located at the  $\alpha/\gamma$  phase boundary have significant detract to strength of Ti-Al polycrystalline.

**Keywords:**  $\alpha + \gamma$  two phase TiAl alloy; void; molecular dynamics

## 1. Introduction

TiAl alloy has been used as structural material in aviation industry because its inherent advantages such as low density and self-diffusion rates, high elastic module and high strength [1]. Two-phase titanium aluminum alloys with proper phase distribution and grain size exhibit better mechanical performance compared with monolithic constituents  $\gamma$ (TiAl) and  $\gamma$ (Ti<sub>3</sub>Al) alloy [2]. Brittle fracture in TiAl alloy strongly affects the safety of fracture of structure like turbo of aircraft engine and combustion generator.

Deformation phenomena in TiAl alloys have been widely studied in order to overcome the problems associated with the limited ductility and damage tolerance. The literature data covers a wide range of parameters such as alloy composition, microstructure and deformation temperature. Much of the work has been performed on single phase  $\gamma$  alloys and PST crystals. Rupture failure at the macroscopic scale can be attributed to nucleation, growth and propagation of cracks, but at the microscopic scale cracks are initially easily formed at defects in the casting process, such as voids and inclusions [3]. These defects are known to play a fundamental role in the deformation of the material. Nucleation, growth and coalescence of voids are deemed as the primary mechanism of ductile material fracture, in which void growth is particularly important. Therefore, it is necessary to study the deformation response of porous materials with the consideration of microstructure evolution.

Brittle fracture in TiAl alloy strongly affects the safety of fracture of structure like turbo of aircraft engine and combustion generator [4]. Defects such as grainboundary, void and segregation plays an significant role in the process of fracture [5]. In order to understanding the mechanism of brittle fracture, multi-scale methods from micro to marco scale have been applied to investigate the behavior of fracture. It's necessary to carefully examine the revolution of defects and its influence on the fracture process at atomic scale. A previous study on void growth in gamma-TiAl single crystal has reveals that void with high volume fraction detracts incipient yield strength [6]. Molecular dynamics(MD method has been use to investigate the evolution of void in materials in nanoscale [7]. The fracture mechanisms

33 in the duplex micro-structure are plasticity induced grain boundary decohesion and cleavage, while  
 34 those in the lamellar microstructure are interface delamination and cracking across the lamellae [].

35 MD simulations has reveals that existence of voids alone may contribute to strain hardening  
 36 because they are barriers to dislocation movement [3]

## 37 2. Molecular Dynamics Simulation

### 38 2.1. Atomic Potential

39 The interaction of particle in the material is determined by interatomic potential. Many reported  
 40 examples of crack propagation in metal materials were performed with embedded atomic method  
 41 due to is better accuracy in metal lattice compare with F-S and L/J []. The embedded atom method  
 42 (MEAM) potential developed by Zope and Mishin by [] was used in the study. The simulation is  
 43 submitted by MD simulations with the Large-scale Atomic/Molecular Massively Parallel Simulator  
 44 (LAMMPS) open-source code []. We performed constant-pressure and constant-temperature (NPT)  
 45 molecular dynamics simulation.

$$E_{total} = \sum F_i(\rho_{h,i}) + \frac{1}{2} \sum_i \sum_{j(\neq i)} \phi_{ij}(R_{ij}) \quad (1)$$

46 where  $E_{total}$  is the total energy of the system,  $\rho_{h,i}$ , is the host electron density at atom  $i$  due to the  
 47 remaining atoms of the system,  $F_i(\rho)$  is the energy for embedding atom  $i$  into the background electron  
 48 density  $\rho$ , and  $\phi_{ij}(R_{ij})$  is the core-core pair repulsion between atoms  $i$  and  $j$  separated by the distance  
 49  $R_{ij}$ . It can be noted that  $F_i$  only depends on the element of atom  $i$  and  $\phi_{ij}$  only depends on the elements  
 50 of atoms  $i$  and  $j$ . The electron density is, as stated above, approximated by the superposition of atomic  
 51 densities, namely

### 52 2.2. Model Creation of Crystalline

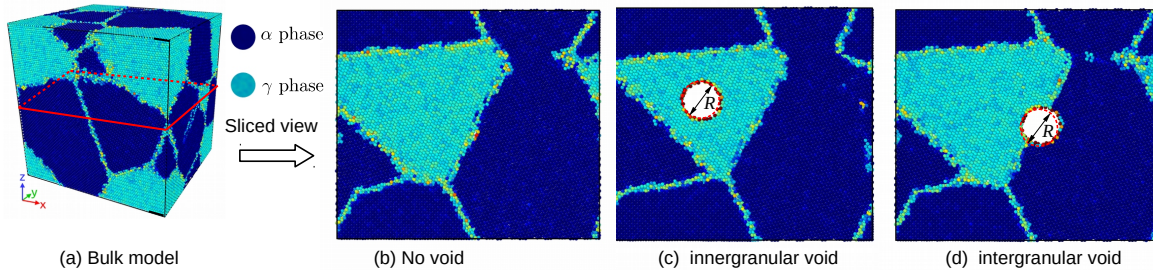


Figure 1. Overview of model creation

53 []  $\gamma$  TiAl has a fcc-centered tetragonal with an  $L1_0$  structure [], and  $\alpha$ TiAl is hcp structure, the  
 54 structure of the two initial cells are shown in Fig.[], and the constructing parameters are given by Table.[].  
 55 The simulation cells of two phase polycrystalline with an initially spherical void at different position  
 56 are shown in figure []. Periodic boundary conditions (PBC) are applied along all three directions, that  
 57 makes poly crystal with periodic nanovoid structures. The initial dimension of simulation cell is  $L_x =$   
 58 nm,  $L_y =$  nm,  $L_z =$  nm, and each model contains about 4.6 million atoms. The grain orientation and  
 59 size were randomly created with Voronoi method with code ATOMSK [], and resulting in the arbitrary  
 60 shape and orientation of the grains. Only one spherical void defect was placed intragranularly or  
 61 intergranularly within each simulation model void within each simulation model. The intragranular  
 62 spherical void was located in grain interior of the largest grain of the simulation model, as shown in  
 63 Fig. []. The intergranular spherical void was at the center of the simulation cell, as shown in Fig. [].

**Table 1.** Parameters of nanocrystalline

Phase	Space group	Designation	Parameters
$\alpha_2$	P6 <sub>3</sub> /mmc	0 <sub>19</sub>	$a = 0.5765$ $c = 0.46833$
$\gamma$	tP4	L1 <sub>0</sub>	$a = 0.3997$ $c = 0.4062$

### 64 2.3. Analysis method

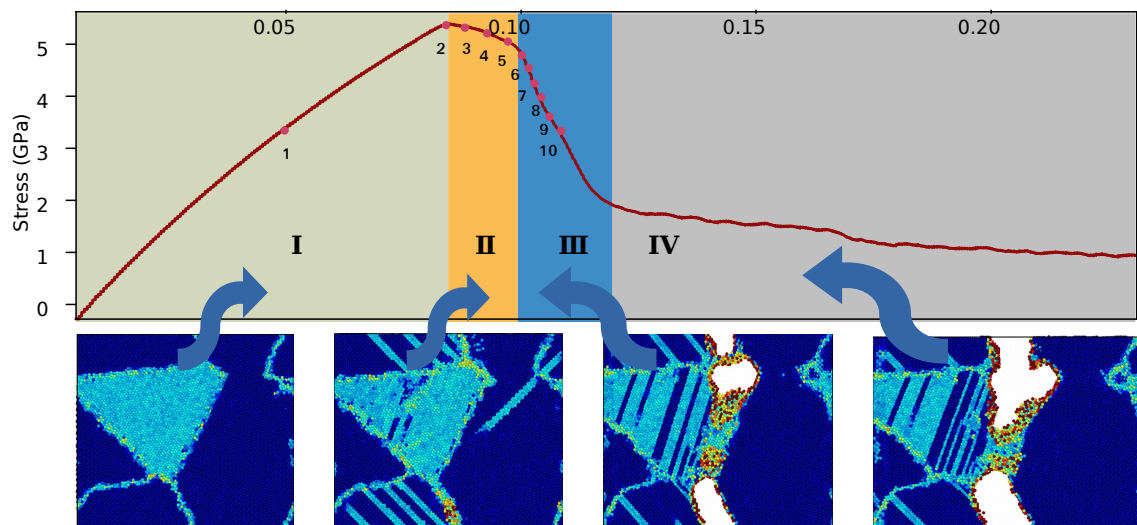
65 The centrosymmetry parameter is defined as follow:

$$P = \sum_{i=1}^6 |\vec{R}_i + \vec{R}_{i+6}|^2 \quad (2)$$

66 where  $\vec{R}_i$  and  $\vec{R}_{i+6}$  are the vectors corresponding to the six pairs of opposite nearest neighbors  
67 in the fcc lattice. The centrosymmetry parameter(CSP) is zero for atoms in a perfect lattice. In other  
68 words, if the lattice is distorted the value of P will not be zero. Instead, the parameter will have a value  
69 within the range corresponding to a particular defect. By removing all the perfect and surface atoms  
70 within the bulk, the existence of dislocation atoms become visible.

### 71 3. Results and Discussion

72 The model without any type of void defect was regarded as benchmark of other simulation,  
73 deformation mechanisms were chosen to . In order to examine deformation behaviour carefully, the  
74 whole tension process was sliced into four stages. Stage 1 is typical elastic stage of the model, which  
75 originates from strain  $\epsilon = 0$  to  $\epsilon = 0.09$ . Stage 2 is yield stage of the model from  $\epsilon = 0.09$  to  
76  $\epsilon = .$  stage 3. cracking stage and 4. Fracture stage. More specifically, a greater number of moments was  
snapped in stage 2 and stage 3.

**Figure 2.** perfect-line2-2

77

**Table 2.** Key point during tensile process

Key Number	1	2	3	4	5	6	7	8	9	10
Time/ps	0	0.15	0.16	0.17	0.18	0.19	0.20	0.21	0.22	0.23
Strain	0	0.15	0.16	0.17	0.18	0.19	0.20	0.21	0.22	0.23

**78 3.1. Deformation Behaviour of Two Phase Alloys without Void Defects**

**79** However, the following discussion concentrates on deformation phenomena that rely on the  
**80** elastoplastic codeformation of the  $\gamma$  and  $\gamma_2$  phases and on the particular point defect situation occurring  
**81** in twophase alloys. Due to this effect ( $\alpha_2 + \gamma$ ) alloys exhibit some remarkable properties that are  
unlike those of either constituent. The configure of atoms is shown in Fig.8, it can be seen that

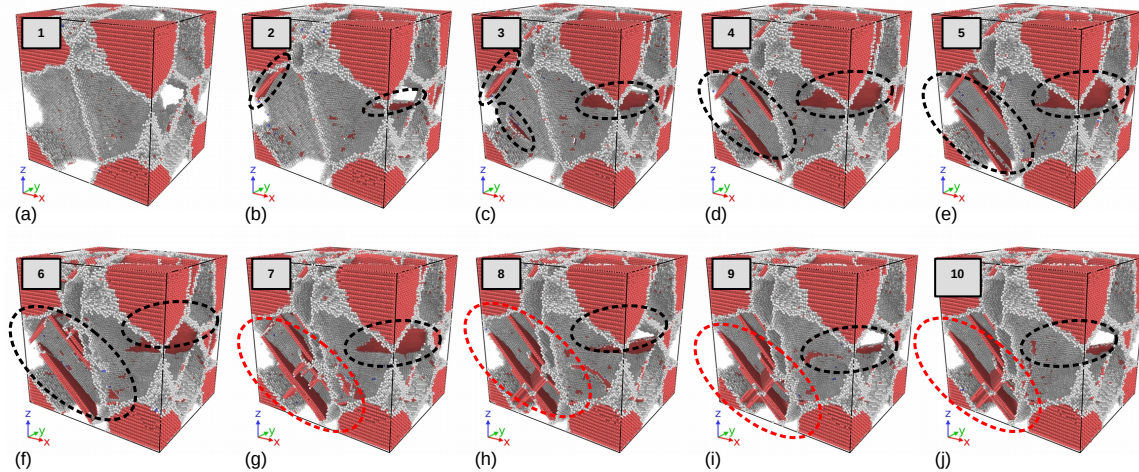


**Figure 3.**  $\gamma$  phase deformation

**82** dislocation emission initiate in  $\gamma$  pahse in XXX ps, and the deformation canbe mainly confied to the  
**83** majority  $\gamma$  pahse.  $\gamma$ (TiAl) deforms by octahedral glide of ordinary dislocations with the Burgers  
**84** vector  $b=1/2<110]$  and superdislocations with the Burgers vectors  $b=<101]$  and  $b = 1/2 < 11\bar{2}]$ . The  
**85** other potential deformation mode is mechanical twinning along  $1/6 < 11\bar{2}]111$ . From Fig.8, of the  
**86** two constituents of  $(\alpha_2+\gamma)$  alloys, the  $\alpha_2$  phase is more difficult to deform. A reason for the unequal  
**87** strain partitioning between the  $\alpha_2$  and  $\gamma$  phase is certainly the strong plastic anisotropy of the  $\alpha_2$   
**88** phase. TEM examinations performed on tensile tested lamellar alloys have revealed that the limited  
**89** plasticity of the  $\alpha_2$  phase is mainly carried by local slip of  $<\mathbf{a}>$ -type dislocations with the Burgers vector  
**90**  $b = 1/3 < 11\bar{2}0 >$  prism planes<sup>8</sup>, which is by far the easiest slip system in  $\alpha_2$  single crystals. Basic

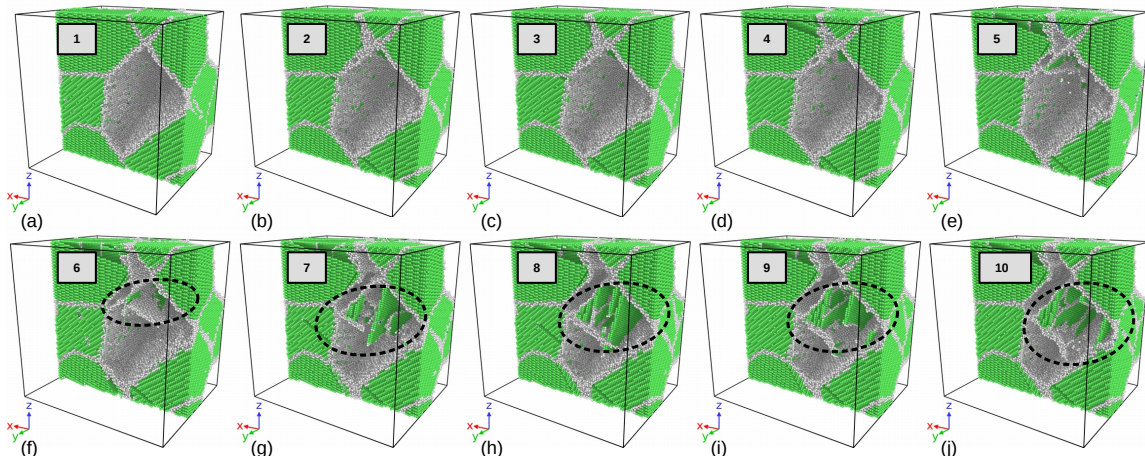


**Figure 4.**  $\alpha$  phase deformation

**91** deformationg mechanism of  $\alpha$  phase

**92** 1.In many cases the orientation of slip slip is changed because the crystallographically available  
**93** slip and directions are not continuous across the interface. This may significantly reduce the Schmid

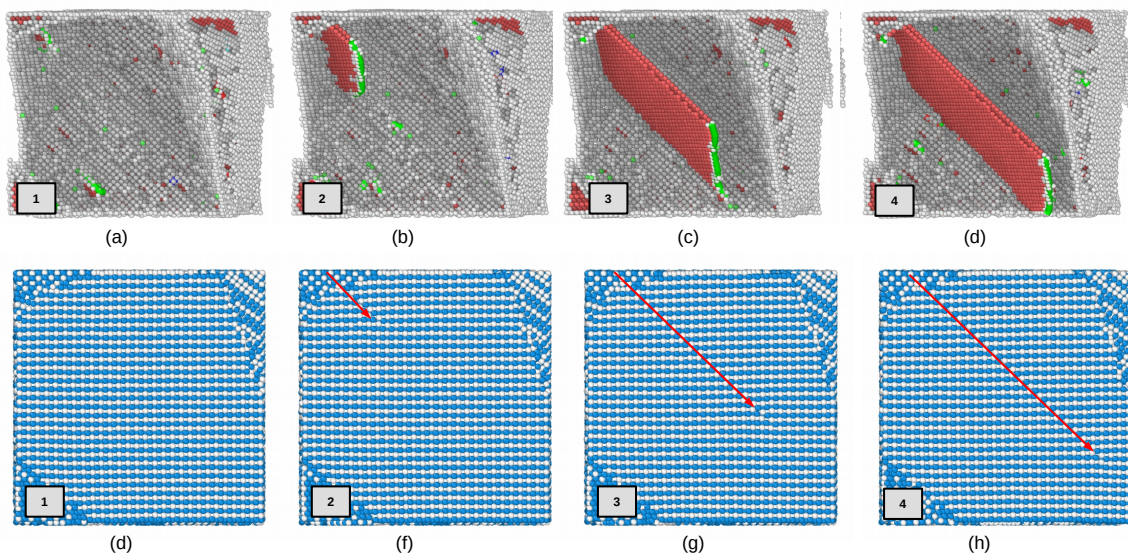


**Figure 5.** Dislocation in  $\gamma$

factor and thus impede slip transfer. At the  $\gamma/\gamma$  interfaces the orientation of the slip plan could change through a relevantly large angle of about 90 degree. Reorientation of slip is always required at the  $\alpha_2/\gamma$  interface; the smallest angle between the corresponding slip planes  $111_\gamma$  and  $10 - 10_{\alpha_2}$  is about 19 degree [1].

The core of a dislocation intersecting an interface often needs to be transformed. For example, an ordinary  $1/2<110]$  dislocation gliding in one  $\gamma$  grain has to be converted in to a  $<101]$  super dislocation with the double Burgers vector gliding in an adjacent  $\gamma$  grain. At the  $\alpha/\gamma$  interface the dislocations existing in the  $D0_{19}$  structure have to be transformed into dislocations consistent with the  $L1_0$  structure. These core transformations are associated with a change of the dislocation line energy because the lengths of the Burgers vectors and the shear module are different.

Dislocations crossing semi-coherent boundaries have to intersect the misfit dislocations, a process that involves elastic interaction, jog formation and the incorporation of gliding dislocations into the mismatch structure of the interface. When the slip is forced to cross  $\alpha_2$  lamella, pyramidal slip of the  $\alpha_2$  phase is required, which needs an extremely high shear stress.

### 3.2. Evolution of spherical void in the simulation with intragranular spherical voids

The volume defects considered pertain to three-dimensional objects contained within a matrix. Three-dimensional structures composed of zero-, one- or two-dimensional defects are not considered here. Second-phase particles, precipitated within, as a consequence of a thermal treatment, or taken up, as a consequence of a material processing route, into a matrix of the first, dominant phase, disrupt, more or less (as possibly associated with the occurrence of incoherent or coherent interfaces; see Sect. 5.3), the long-range translation symmetry of the matrix. They may induce considerable misfit-stress fields and thus can influence material properties pronouncedly. Such stress fields surrounding the second-phase particles can be due to misfit between the volume occupied by the second-phase particle when unconstrained and the space ("hole") put at its disposal by the matrix. Such misfit can arise due to specific volume differences induced by precipitation or by different thermal expansion or shrinkage upon heating or cooling the specimen. A possibly favourable effect of second-phase particles is a contribution to the enhancement of mechanical strength. Considering yielding of a material as related to glide of dislocations (Sect. 5.2.5), any mechanism obstructing dislocation glide improves the mechanical strength. In the discussion of the Frank–Read source for dislocation (-line) production (Sect. 5.2.6) it was made clear that second-phase particles can serve as obstacles for dislocation migration: the stress fields surrounding the second-phase particles can be of "antagonistic" nature and "block"

propagation of the stress field of a migrating dislocation: the second-phase particle acts as “pinning point”. It was already indicated that in order that a dislocation can pass two pinning points (A and B in Fig. 5.13; see Sect. 5.2.6) a critical shear stress is needed that depends on the distance between the obstacles (which can be second-phase particles):

$$\tau_0 = Gb/d \quad (3)$$

where  $d$  represents the distance between A and B and thus reflects the dependence of the critical shear stress  $\tau_0$  on the second-phase particle density and distribution. This mechanism for hardening is designated as the Orowan process (with  $\tau_0$  as the Orowan (shear) stress ; sgitee also Sect. 11.14.4). As a result of the Orowan process, upon passage of the pinning points by a series of gliding dislocations, a system of concentric loops is formed around the second-phase particles (see Fig. 5.27). Consequently, the effective average distance between the second-phase particles has decreased to  $d$  which implies a necessary increase of the value of critical shear stress required for continuation of dislocation glide (cf. (5.10)). A step, of the width of a burgers vector, will be generated at both sidesof a crystal along teh direction of teh burgers vector after dislocation traversing teh entire crystal, as is shown in ???. A small step will be formed at spherical void surface toward teh void interiorafter dislocation absorbtionat sphericalvoid surfaces, as is shown in ???. If a great number of dislocation slip along their respective systemstowards teh spherical nanovoid in all directions, and are absorbed at spherical void surfaces, the spherical nanovoid will eventually shrink from teh dash circle to

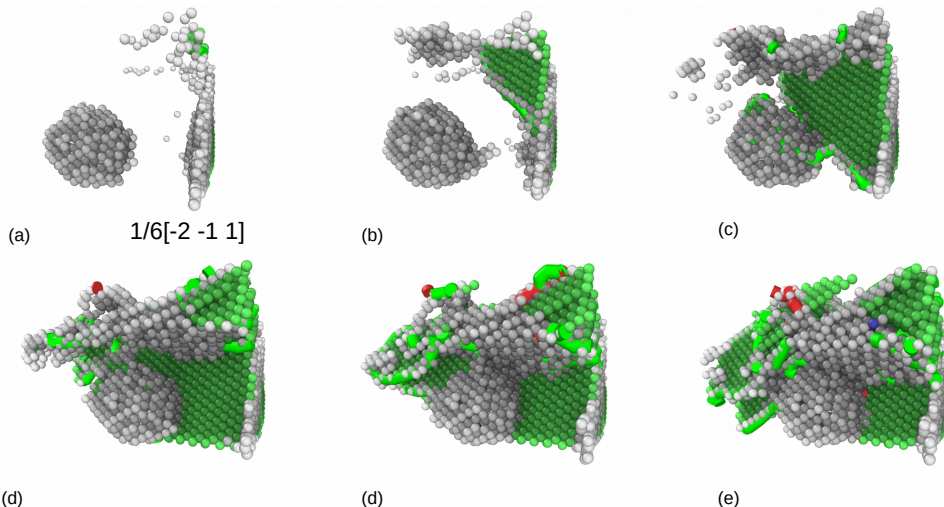


**Figure 6.** Dislocation around void

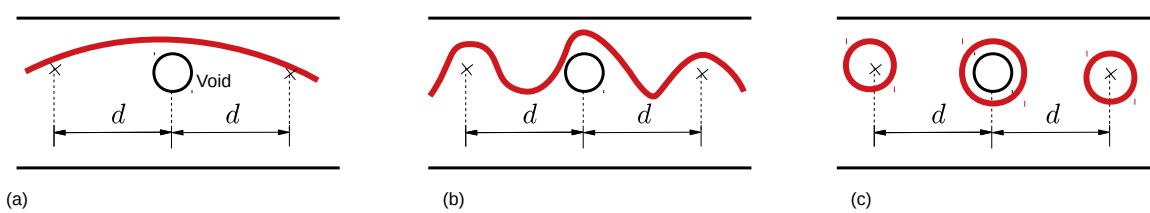


**Figure 7.** orowan

### 123 3.3. The effect of void on the strength of material

124 Void of R=10 was placed at phase boundary, inside  $\alpha$  phase grain respectively. Effect of void at  
125 different position under uniaxial tension is shown in Fig.9. The strength of materials with void in  
126 different size and at different position is shown in Fig.9. The results show that the model without void

defect has best strength, while the void located inside  $\alpha$  phase detracts the strength of the material most, and the void at the phase boundary have less impact on the strength.

The effect of size is expectable that the greater voids detracts the strength of the materials more, however, it has been observed in the simulation that there is a critical value about 15A for voids at different position. The voids larger than 15 A have dramatic detraction to the strength of the material. Conventional definition of strength of materials with geometry subtraction was applied to the model, and theoretical strength of the models was calculated by formulation 4:

$$\sigma^* = \sigma_0 \cdot \frac{A^*}{A_0} \quad (4)$$

where  $\sigma_0$  is the strength of the model without void defects 5.26 Gpa, and  $A_0$  is initial section area,  $A = a \times b = 36000A^2$ ,  $A^*$  is section area in consider of the subsection that results from the voids. Comparing with the strength determined by molecular dynamics simulation and the results calculated with formulation 4, it can be assumed that the main factor that affects the strength of materials can be attributed to local behaviour of the materials, thus evolution of defects should be examined carefully.

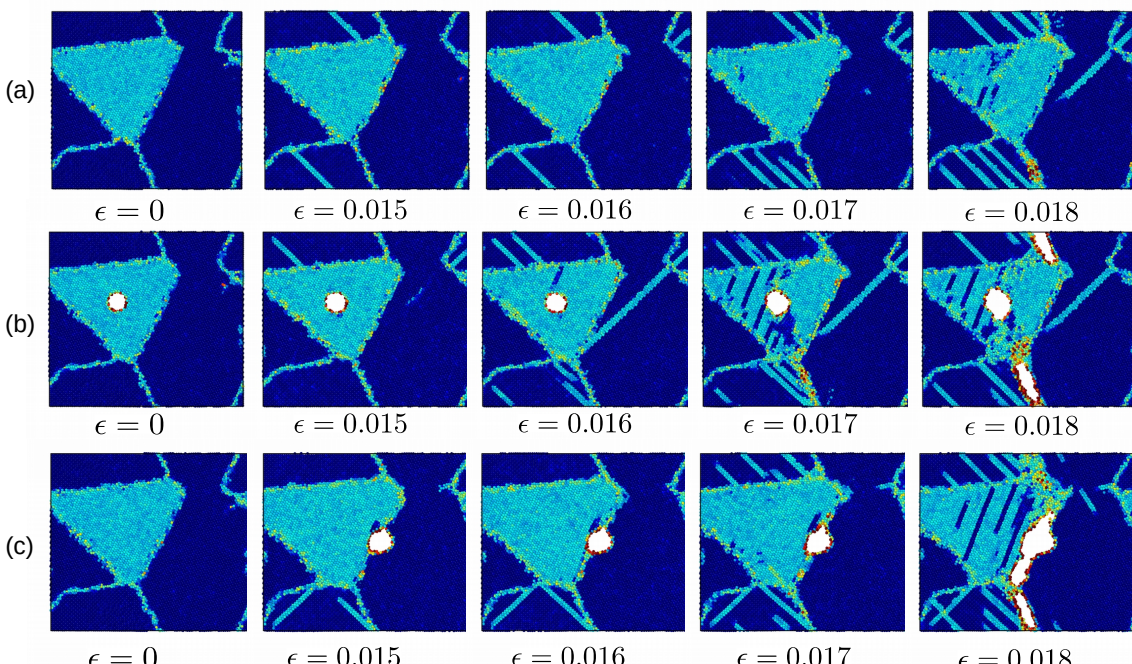


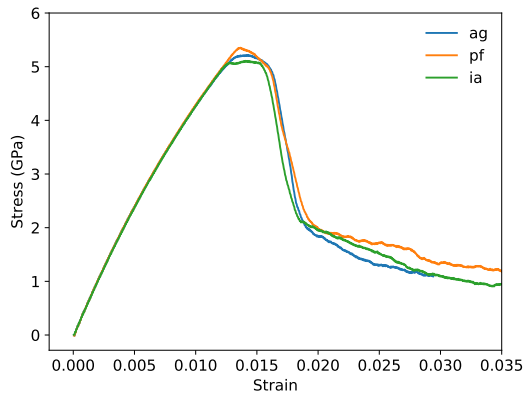
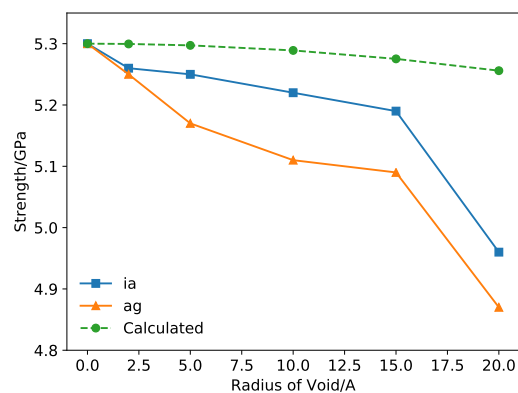
**Figure 8.** Yield process of the models

Voids with different size: 2A, 5A, 10A, 15A were placed into the model respectively. It has been observed that voids detracts the strengths of the material. The max stress stress of the simulation cell decreases as the volume of voids are larger. From Fig ??, there is a critical value of void radius about 15A, the void greater than 15A cause serious detraction of strength of material. Engineering stress is calculated

$$\sigma = S/A$$

The rate of decrease of loading area are smaller comparing with the detraction of strength, so it can be assumed that the yield behaviour and strength is much more related with local behaviour of grain boundaries and void.

Grain and phase boundaries are obstacles to deformation process, thus the stability of boundaries have great impact on the strength of materials. Interaction between grainboundary and void determines the fracture mode of the TiAl alloy.

**Figure 9.** Stress-Strain**Figure 10.** Strength of models

According to Schmid's law:

$$\tau = \sigma * m$$

where m is the Schmid factor :

$$m = \cos(\phi)\cos(\lambda)$$

145

#### 146 References

1. Vu, T.T.T.; Zehender, T.; Verheijen, M.A.; Plissard, S.R.; Immink, G.W.G.; Haverkort, J.E.M.; Bakkers, E.P.A.M. High optical quality single crystal phase wurtzite and zincblende InP nanowires. *Nanotechnology* **2013**, *24*, 115705. doi:10.1088/0957-4484/24/11/115705.
2. Kim, Y.W. Effects of microstructure on the deformation and fracture of  $\gamma$ -TiAl alloys. *Materials Science and Engineering: A* **1995**, *192-193*, 519–533. doi:10.1016/0921-5093(94)03271-8.
3. Xiong, L.; Xu, S.; McDowell, D.L.; Chen, Y. Concurrent atomistic-continuum simulations of dislocation-void interactions in fcc crystals. *International Journal of Plasticity* **2015**, *65*, 33–42. doi:10.1016/j.ijplas.2014.08.002.

154 © 2018 by the authors. Submitted to *Journal Not Specified* for possible open access  
155 publication under the terms and conditions of the Creative Commons Attribution (CC BY) license  
156 (<http://creativecommons.org/licenses/by/4.0/>).